

## Raudel Avila

Department of Mechanical Engineering,  
Northwestern University,  
Evanston, IL 60208  
e-mails: roavila@u.northwestern.edu;  
raudelavila2023@u.northwestern.edu

## Joanna L. Ciatti

Department of Materials Science and Engineering,  
Querrey Simpson Institute for Bioelectronics,  
Northwestern University,  
Evanston, IL 60208  
e-mail: jciatti@u.northwestern.edu

## Abraham Vázquez-Guardado

Querrey Simpson Institute for Bioelectronics,  
Center for Bio-Integrated Electronics,  
Northwestern University,  
Evanston, IL 60208  
e-mail: abraham.vg@northwestern.edu

## Yixin Wu

Department of Materials Science and Engineering,  
Querrey Simpson Institute for Bioelectronics,  
Northwestern University,  
Evanston, IL 60208  
e-mail: yixinwu2017@u.northwestern.edu

## Yamin Zhang

Querrey Simpson Institute for Bioelectronics,  
Center for Bio-Integrated Electronics,  
Northwestern University,  
Evanston, IL 60208  
e-mail: yamin.zhang@northwestern.edu

## Rinaldo Garziera

Dipartimento di Ingegneria ed Architettura,  
Università di Parma,  
Parma 43121, Italy  
e-mail: rinaldo.garziera@unipr.it

## John A. Rogers

Querrey Simpson Institute for Bioelectronics,  
Center for Bio-Integrated Electronics,  
Department of Mechanical Engineering,  
Department of Materials Science and Engineering,  
Department of Biomedical Engineering,  
Department of Electrical and Computer  
Engineering,  
Department of Chemistry,  
Department of Neurological Surgery,  
Northwestern University,  
Evanston, IL 60208  
e-mail: jrogers@northwestern.edu

# Electrochemical Bioelectronics in Drug Delivery: Effect of the Initial Gas Volume

*Implantable bioelectronic devices with drug delivery capabilities have emerged as suitable candidates for biomedical applications focusing on localized drug delivery. These classes of miniaturized bioelectronics offer wireless operation and refillable designs that can be used for repeated animal behavioral studies without restricting their motion. The pumping mechanisms of these bioelectronic devices features soft materials, microfluidics, and electrochemical subsystems that can be scaled from behavioral studies in small animals to delivery of life-saving medication in humans. Here, we study the refillable aspect of these bioelectronic systems using an analytic model for the drug delivery time established from the ideal gas law when an initial gas volume is present in the device electrolyte reservoirs. The effect of the initial gas volume in delaying the drug delivery time is captured via a non-dimensional parameter identified as the normalized initial gas volume. An analytical solution is derived from the perturbation method, which agrees well with the numerical solution. These results have relevance in the reusability aspect of these bioelectronic systems since modifying the amount of initial gas in the device reservoirs for different experiments affects the total delivery time and can serve as a tunable parameter to ensure timely and successful delivery of the drug in the target region. [DOI: 10.1115/1.4052883]*

*Keywords: implantable bioelectronics, electrochemical reaction, drug delivery, ideal gas law, flexible membrane, analytical model, mechanical properties of materials*

<sup>1</sup>Corresponding author.

Contributed by the Applied Mechanics Division of ASME for publication in the JOURNAL OF APPLIED MECHANICS. Manuscript received October 13, 2021; final manuscript received October 27, 2021; published online November 18, 2021. Assoc. Editor: Pradeep Sharma.

## 1 Introduction

Recently developed miniaturized, refillable, and implantable bioelectronic devices with drug delivery capabilities have enabled localized drug delivery to organs/tissues without restricting the movement of small animals and avoiding excessive heat that can alter the drug properties and animal behavior [1–8]. Technologies to deliver drug locally can range from nanoparticles to implantable microneedles [9] to sophisticated bioelectronics with fluidic microsystems [6,8,10–12] that aim deliver the drug directly to the target area to enhance its effect. Delivering the drug locally offers certain advantages over a systemic delivery approach—where the drug must travel through the body to reach the target location—since interactions with other biological tissues and unwanted side effects can be potentially avoided [9,13,14]. Specifically, implantable bioelectronic devices have been used for localized delivery in the brain [5] and peripheral nerves [4] in the context of neuroscience research [15] and cancer therapeutics [16–18]. The schematic and components of a typical implantable bioelectronic device used for localized delivery studies is shown in Fig. 1. This design features two refillable reservoirs: (1) electrolyte and (2) drug. In the partially filled electrolyte reservoir, a set of interdigitated electrodes—in direct contact with the liquid electrolyte—initiate an

electrochemical reaction (e.g., water hydrolysis) to generate gas when electric current flows through them. The gas generation (illustrated via bubble formation in Fig. 1(b)) pressurizes the electrolyte reservoir, which is only partially filled with the liquid electrolyte leaving an initial gas volume  $V_0$  to deform a flexible membrane; the deformation transitions from bending dominated (small deformation) to stretching dominated (finite deformation) [19,20], where the flexible membrane adopts the shape of a spherical cap (like the drug reservoir). As the flexible membrane deforms, the drug (located on top of the flexible membrane in the drug reservoir) is pushed through a network of microfluidic channels into the target location inside the body [21–23]. Let  $V$  denote the volume of gas due to electrochemical reaction such that the total volume of gas in the electrolyte reservoir is  $V + V_0$ .

The mechanics of drug delivery in these microsystems is influenced by environmental, microfluidic, flexural, electrochemical, and geometrical parameters totaling approximately 12 individual parameters (ten are shown in Fig. 1, the remaining two are flexural parameters listed below). These parameters include the initial environmental pressure at the target organ/tissue  $P_0$  that varies depending on the internal pressure of the organ/tissue (e.g., eye, blood, brain, lungs) [24], the microchannel length  $L$  and cross-sectional dimensions  $a$  and  $b$  [25], the drug viscosity  $\mu$ , the flexible membrane thickness  $h$  and radius  $R_0$  as well as flexural parameters such as the Young's modulus  $E$ , Poisson's ratio  $\nu$ , and the constitutive stress–strain relationship  $\sigma - \epsilon$  [20,26,27]. Inside the partially filled electrolyte reservoir, the liquid electrolyte temperature  $T$  and electrical current  $i$  flowing in the electrodes influence the gas generation dynamics [22]. Most importantly, for the analysis in this article, the presence of an initial gas volume  $V_0$  when the electrolyte reservoir is only partially filled with the liquid electrolyte (shown in blue in Fig. 1(a)). This initial gas volume  $V_0$  and volume of the liquid electrolyte add to the constant volume of the electrolyte reservoir.

This electrochemical actuation principle and bioelectronic device form factors used in small animal experiments can be scaled up for drug delivery studies in larger animals, and in the future, human applications. During experimental trials, controlling the parameters that influence the drug delivery process yield insights of the total delivery time and volume temporal profile, and both are keys to ensure timely and successful delivery. To that end, a scaling law that combines all the environmental, microfluidic, flexural, electrochemical, and geometrical terms into two nondimensional parameters (one for the environmental pressure and the other for the microfluidic resistance) has been previously established [28] to model and optimize the drug delivery process when the flexible membrane is modeled as a Marlow hyperelastic material [29] under finite deformation. The scaling law, and analytical solution obtained using the perturbation method, neglects the effect of the initial gas volume present at the beginning of the delivery, i.e., the electrolyte chamber is completely full of the liquid electrolyte [28]. However, when considering the refillable capabilities of these devices [4,5], the presence of an initial gas volume  $V_0$  in

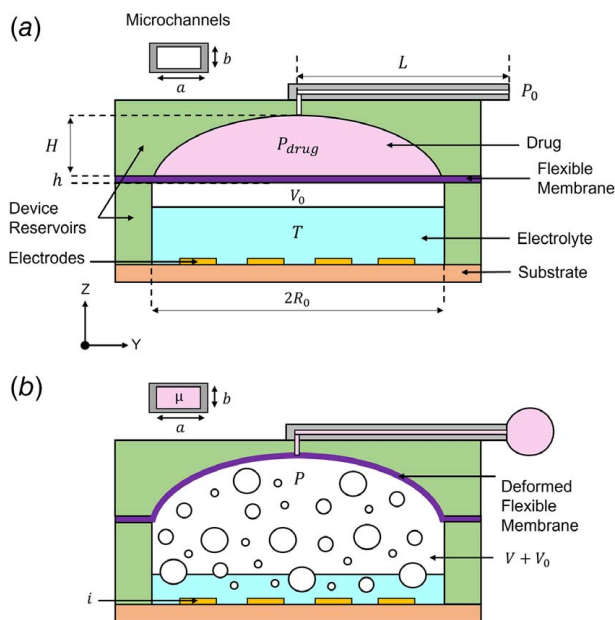


**Fig. 1 Schematic of electrochemical bioelectronics used in drug delivery. (a) Electrolyte reservoir is partially filled where an initial volume of gas is present. (b) The gas formation process deforms the flexible membrane to pump the drug from inside the device into the target location.**

the electrolyte chamber must be accounted for as it affects the drug delivery. For a partially full electrolyte chamber (Fig. 1(a)), the presence of an initial gas volume  $V_0$  will slow down the drug delivery process. Therefore, studying the effect of  $V_0$  in the total delivery time can yield an additional parameter that can be tuned to control the drug delivery process on clinically relevant settings.

Here, we propose a modified scaling law that accounts for the effects of the initial gas volume and obtain a new analytical solution using the perturbation method [30], validated by the numerical results, that can be used to control the drug delivery process using three nondimensional parameters. The drug volume temporal profile is used to determine the drug delivery time for bioelectronic devices of different sizes that correspond to representative applications in small animals, large animals, and humans.

The organization of this article is as follows. First, the Mooney Rivlin [27] hyperelastic strain energy potential is used for the flexible membrane mechanics analysis in Sec. 2. Then, scaling law of drug delivery that accounts for the effect of the initial gas volume in the electrolyte chamber is derived and solved analytically using the perturbation method in Sec. 3. The validation and the parametric study of the drug delivery time for different initial gas volumes is discussed in Sec. 4, where designs sizes for small animals, large animals, and human applications are presented. Finally, alternative material models are presented to highlight the sensitivity of the analytical model to the mechanics of the flexible membrane.

## 2 Mechanics of the Flexible Membrane—Mooney Rivlin Solid

The function of the flexible membrane is to respond to an asymmetric pressure stimulus from inside the device electrolyte reservoir, which results in hydraulic power to pump the drug into the target location through the microchannels. This pumping mechanism is achieved by a pressure difference  $P - P_{\text{drug}}$ , where  $P$  is the gas pressure generated from the electrochemical reaction and  $P_{\text{drug}}$  is the pressure from the drug on top of the flexible membrane. Before the drug delivery process begins, the pressures are at equilibrium, i.e.,  $P = P_{\text{drug}} = P_0$ .

For a circular flexible membrane of radius  $R_0$ , thickness  $h$ , the pressures  $P$  and  $P_{\text{drug}}$  on its two sides drive the membrane deformation whose displacement induces a volume  $V$  given by

$$P - P_{\text{drug}} = f(V) \quad (1)$$

where the function  $f(V)$  depends on  $R_0$ ,  $h$ , and the hyperelastic strain energy potential typically used to model nonlinear elastic and incompressible materials [29] (e.g., Neo-Hookean, Mooney Rivlin, Yeoh, Ogden, Marlow, among others). For a linear-elastic material and infinitesimal deformation such that the maximum deflection  $H \ll h$  ( $h$ —membrane thickness), the deformation of polymer membrane is bending-dominated and can be modeled as an linear elastic thin plate [26], which yields the function  $f(V) =$

$\frac{16Eh^3}{\pi R_0^6(1-\nu^2)}V$  [19,28]. For large deflection ( $H \gg h$ ) such that the deformation is stretching dominated and the membrane deforms to a spherical cap under uniform pressure, Our previous work [28] gives  $f(V)$  analytically for the Marlow hyperelastic potential [27] but did not account for the effect of initial gas volume. For intermediate deflection ( $H \sim h$ ),  $f(V)$  can be obtained numerically by the finite element method [4,19]. In the following, we use the Mooney-Rivlin hyperelastic potential as an example to derive  $f(V)$  for large deflection, accounting for the effect of initial gas volume, and this approach can be straightforwardly extended to any other hyperelastic potentials. The complete derivation of  $f(V)$  is presented here for the sake of completeness. The above three scenarios can be equivalently expressed in terms of the drug volume  $V$

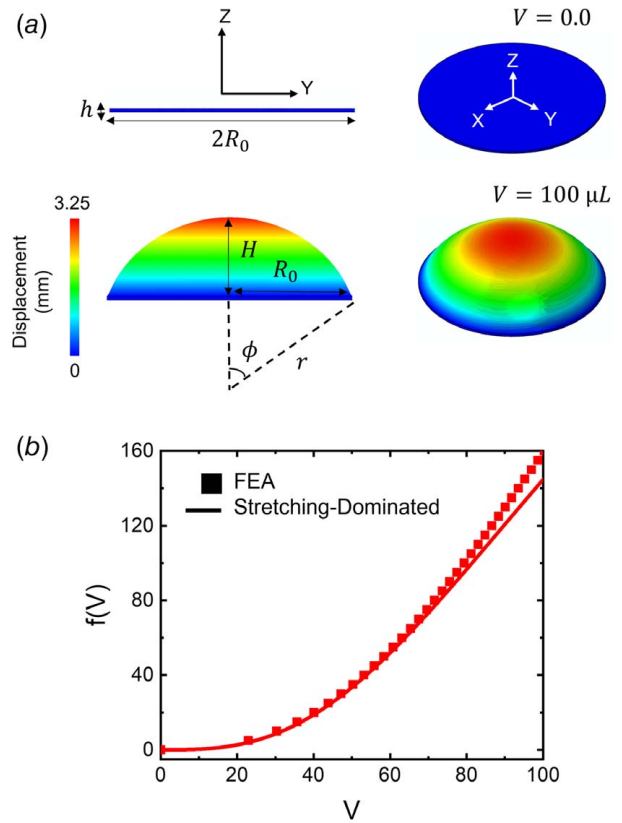


**Fig. 2 Flexible membrane mechanics during deformation. (a) FEA results for the displacement of a flexible membrane as it deforms into the shape of a spherical cap with a target delivery volume of  $V = 100 \mu\text{L}$ . The maximum displacement is given by  $H$ . The flexible membrane dimensions are  $R_0 = 5 \text{ mm}$  and  $h = 0.15 \text{ mm}$ . (b) Function  $f(V)$  for the flexible membrane modeled as a Mooney Rivlin incompressible solid.**

as follows:

$$V \ll \frac{\pi h R_0^2}{3} \quad \text{for } H \ll h \quad (2)$$

$$\sim \frac{\pi h R_0^2}{3} < V < \sim \frac{\pi h}{6} (3R_0^2 + h^2) \quad \text{for } H \sim h \quad (3)$$

$$V \gg \frac{\pi h}{6} (3R_0^2 + h^2) \quad \text{for } H \gg h \quad (4)$$

For  $H \gg h$  or equivalently drug volume  $V \gg \frac{\pi h}{6} (3R_0^2 + h^2)$  as shown in Eq. (4), the effect of bending deformation (particularly near the clamped edge of the flexible membrane) is negligible such that the deformed shape is a spherical cap, characterized by the spherical angle  $\phi$  that tracks the deformation of the membrane from flat into the shape of a spherical cap as shown in Fig. 2(a).

The maximum height  $H$  of the deformed flexible membrane is related to  $\phi$  as follows:

$$H = (1 - \cos \phi) \frac{R_0}{\sin \phi} \quad (5)$$

The volume of the spherical cap can be expressed in terms of  $\phi$  as follows:

$$V = \frac{1}{6} \pi H (3R_0^2 + H^2) = \frac{\pi R_0^3}{6} \frac{1 - \cos \phi}{\sin \phi} \left[ 3 + \left( \frac{1 - \cos \phi}{\sin \phi} \right)^2 \right] \quad (6)$$

which gives the parametric equation for the volume. The pressure difference  $P - P_{\text{drug}}$  on the two sides of the membrane balance the stress traction as follows:

$$\pi R_0^2 (P - P_{\text{drug}}) = 2\pi\sigma h' R_0 \sin \phi \quad (7)$$

where  $\sigma$  is the true stress under equibiaxial stretching. The membrane thickness due to material incompressibility is  $h' = \frac{\sin^2 \phi}{\phi^2} h$ . Rearranging Eq. (7) yields the general analytic, but parametric expression for the pressure difference  $P - P_{\text{drug}}$  as follows:

$$P - P_{\text{drug}} = f(V) = \frac{2h \sin^3 \phi}{R_0 \phi^2} \sigma(\phi) \quad (8)$$

where the true stress  $\sigma(\phi)$  depends on the adopted material model. For the Mooney Rivlin incompressible hyperelastic potential, the equibiaxial stress at the edge of the membrane is given by [19,27,28]

$$\sigma(\phi) = \frac{4E}{15} \left[ \left( \frac{\phi}{\sin \phi} \right)^2 - \left( \frac{\sin \phi}{\phi} \right)^4 \right] - \frac{E}{15} \left[ \left( \frac{\sin \phi}{\phi} \right)^2 - \left( \frac{\phi}{\sin \phi} \right)^4 \right] \quad (9)$$

Substituting Eq. (9) into Eq. (8) then yields

$$f(V) = \frac{4Eh \sin^3 \phi}{3R_0 \phi^2} \left\{ \frac{2}{5} \left[ \left( \frac{\phi}{\sin \phi} \right)^2 - \left( \frac{\sin \phi}{\phi} \right)^4 \right] - \frac{1}{10} \left[ \left( \frac{\sin \phi}{\phi} \right)^2 - \left( \frac{\phi}{\sin \phi} \right)^4 \right] \right\} \quad (10)$$

Together, Eqs. (6) and (10) are the analytic, but parametric, equations for the function  $f(V)$  for a Mooney Rivlin incompressible solid.

Figure 2(a) shows the vertical displacement of a flexible membrane with dimensions  $R_0 = 5$  mm and  $h = 0.15$  mm to illustrate the deformation (from flat to spherical cap) during the drug delivery process. The function  $f(V)$  obtained from finite element analysis (FEA) agrees well (Fig. 2(b)) with the analytical, but parametric, equations for volume and pressure in Eqs. (6) and (10) and validates the analytic model for the Mooney Rivlin hyperelastic potential.

### 3 Mechanics of Drug Delivery—Effect of Initial Gas Volume

The drug delivery process is influenced by the subsystems within the implantable bioelectronic device shown in Fig. 1: (1) electrochemical, (2) flexible membrane (solids), and (3) the microfluidic channels (fluids). Each subsystem contributes to the total delivery time by affecting either the time required for the flexible membrane to overcome the external environmental pressure, the time required for the drug to travel through the network of microchannels, or both. In our previous work [28], a scaling law of the delivery was developed, but the influence of the initial amount of gas  $V_0$  was not considered since the electrolyte chamber was assumed to always be full before the chemical reaction initiates. However, for repeated studies enabled by the refillable capability of the bioelectronic device, the electrolyte chamber can be partially filled with electrolyte thus leaving an initial amount of gas  $V_0$  (as shown in Fig. 1) that will affect the drug delivery dynamics. The hydrogen  $H_2$  and oxygen  $O_2$  gas generated during the electrochemical reaction can be modeled from the ideal gas law [31] as follows:

$$P(V + V_0) = nRT \quad (11)$$

where  $P$  is the pressure,  $V$  is volume change inside the electrolyte reservoir,  $R$  is the ideal gas constant ( $8.3144$  J mol<sup>-1</sup> K<sup>-1</sup>),  $T$  is

the temperature of the electrolyte,  $n$  is the number of moles, the gas generation rate in the electrolyte follows from the Nernst equation [32] and is linearly proportional to the electrical current  $i$  by  $\frac{dn}{dt} = \frac{3i}{4F}$  [21,22,31] for water, and  $F$  is Faraday's constant ( $96,485$  C mol<sup>-1</sup>). The ideal gas law is a reasonable assumption to approximate the physics of the system, but it has limitations at high pressures where the intermolecular forces become relevant. To account for these effects, the Van der Waals equation [33]—which includes molecular size, intramolecular forces, and volume correction terms—can be used instead to fit the behavior of the real gas if the experimental observations and the modeling have large errors.

Before any electrical current  $i$  is applied to electrodes (i.e.,  $t = 0$ ),  $n$  has an initial value of  $n_0$  to satisfy Eq. (11) equation due to the presence of an initial amount of gas  $V_0$  as follows:

$$n = \frac{3i}{4F} t + n_0 \quad (12)$$

The pressure obtained from equilibrium in the subsystems combines both the net pressures at both sides of the flexible membrane  $P - P_{\text{drug}} = f(V)$  in Eq. (1) and the microchannels and the environmental pressure  $P_{\text{drug}} - P_0 = \frac{12\mu L \dot{V}}{ab^3(1 - 0.63 \frac{b}{a})}$  [25] to give

$$P = f(V) + P_0 + \frac{12\mu L \dot{V}}{ab^3 \left( 1 - 0.63 \frac{b}{a} \right)} \quad (13)$$

where  $P_0$  is the initial environmental pressure at the target region ( $\sim 101.3$  kPa for environmental pressure; but can be adjusted accordingly depending on the specific organ/tissue, e.g.,  $\sim 117$  kPa when considering blood pressure [24]),  $\mu$  is the dynamic viscosity of the drug,  $L$  is the length of the microchannels,  $a$  and  $b$  are the width and height of the rectangular microchannel, respectively, and  $\dot{V}$  is the drug flowrate. In the microchannels, the hydrostatic pressure is negligible and therefore not considered in the model since the drug travels in plane at the top of the device before exiting the microchannels into the target location. For a square microfluidic channel (i.e.,  $a = b$ ), the flow resistance term simplifies to  $\sim \frac{32\mu L}{a^4} \dot{V}$ . The initial value of gas substance  $n_0$  is determined from Eqs. (12) and (13) by substituting into Eq. (11) at the time before the delivery:

$$n_0 = \left( P_0 + \frac{32\mu L}{a^4} \dot{V} \Big|_{t=0} \right) \frac{V_0}{RT} \quad (14)$$

Substituting Eqs. (12)–(14) into the ideal gas law Eq. (11) yields a first-order ordinary differential equation (ODE) for the drug volume  $V$  as follows:

$$t = \frac{4F}{3iRT} \left\{ P_0 V + f(V)(V + V_0) + \frac{32\mu L}{a^4} [\dot{V}(V + V_0) - \dot{V}|_{t=0} V_0] \right\} \quad (15)$$

It includes the initial gas volume  $V_0$ , which was previously unaccounted.

Normalizing the volume and time variables as follows:

$$V^* = \frac{V}{R_0^3} \quad (16)$$

$$t^* = t \left( \frac{3RT}{4F} \frac{i}{EhR_0^2} \right) \quad (17)$$

and writing the function  $f(V)$  nondimensionally as follows:

$$G(V^*) = \frac{R_0}{Eh} f(V^* R_0^3) \quad (18)$$

yields a nondimensional ODE:

$$t^* = P_0^* V^* + G(V^*)(V^* + V_0^*) + M^* \left[ \frac{dV^*}{dt^*} V^* + V_0^* \frac{dV^*}{dt^*} \right]_{t^*=0} V_0^* \quad (19)$$

that involves three nondimensional parameters, namely, the initial environmental pressure  $P_0^*$ , the initial volume  $V_0^*$ , and the microfluidic resistance  $M^*$  defined as follows:

$$P_0^* = \frac{R_0}{Eh} P_0 \quad (20)$$

$$V_0^* = \frac{V_0}{R_0^3} \quad (21)$$

$$M^* = \frac{24\mu L RT}{a^4 F} \frac{R_0^2}{E^2 h^2} i \quad (22)$$

The three nondimensional parameters in Eqs. (20)–(22) combine all the relevant parameters ( $\sim 12$ ) of the bioelectronic device shown in Fig. 1 and can be analyzed separately to understand their effect in the drug delivery process.

For negligibly small microfluidic flow resistance  $M^* \sim 0$ , Eq. (15) becomes [19]

$$t = \frac{4F}{3iRT} [P_0 V + f(V)(V + V_0)] \quad (23)$$

which gives the drug delivery time  $t$  in terms of the drug volume  $V$ . In general, the microfluidic flow resistance is not zero but small ( $M^* \ll 1$ ) [19,28] such that the perturbation method is used:

$$t = \frac{4F}{3iRT} [P_0 V + f(V)(V + V_0)] + M^* \bar{t} + O(M^{*2}) \quad (24)$$

Substitution of the above equation into Eq. (15) yields the solution for  $\bar{t}$ ; therefore, the final expression of drug delivery time  $t$  in terms of drug volume  $V$  is expressed as follows:

$$t = \frac{4F}{3iRT} [P_0 V + f(V)(V + V_0)] + \frac{32\mu L}{a^4} \left[ \frac{V + V_0}{P_0 + f(V) + f'(V)(V + V_0)} - \frac{V_0}{P_0 + f'(0)V_0} \right] \quad (25)$$

It degenerates to the analytic model proposed in Ref. [28] for  $V_0 = 0$ . Equation (25) includes two terms; the first term, which is inversely proportional to electrical current  $i$  (and temperature  $T$ ) but independent of microchannel sizes ( $L$  and  $a$ ) and drug viscosity ( $\mu$ ), represents the time required for the flexible membrane to overcome the external environmental pressure  $P_0$  and deform to the desired volume  $V$  given by the drug reservoir shaped like a spherical cap. The last term on the right-hand side, which is linearly proportional to drug viscosity ( $\mu$ ) (and microchannel sizes  $L$  and  $a^{-4}$ ) but independent of electrical current  $i$  (and temperature  $T$ ), is the time required for the total drug volume to travel through the microchannels. The two terms in Eq. (25) occur simultaneously, i.e., as the flexible membrane deforms is pushing the drug through the microchannels, to give the total drug delivery time.

## 4 Results and Discussion

The volume temporal profile provides valuable insights to understand, and optimize, the drug delivery process. This temporal quantity is affected by the three non-dimensional parameters  $M^*$ ,  $P_0^*$ , and  $V_0^*$ , which must be carefully selected to ensure timely and safe (i.e., no damage to surrounding tissues) delivery. The scalability of the microsystem design allows us to analyze (non-dimensionally) the effect of  $V_0^*$  (by fixing  $M^*$ ,  $P_0^*$ ) in the context of the drug volume temporal profiles and apply these findings to bioelectronic devices

**Table 1 Properties and representative values of parameters used in the numerical and analytical models**

Parameter	Small devices	Medium devices	Large devices	Units
$R_0$	1.5	5	10	mm
$E$		15		MPa
$h$		150		$\mu\text{m}$
$T$		310 (core body temperature)		K
$i$	1	10	35	mA
$a, b$		20–200		$\mu\text{m}$
$L$		10		mm
$\mu$		0.89		mPa-s

intended for small or large animal models, and ultimately humans. The following terminology is adopted in this section:

- The term “numerical” is used for solutions of the ODE (Eq. (19)) described in Sec. 3 when the non-dimensional function  $G(V^*)$  is obtained from FEA using the Mooney Rivlin hyperelastic potential.
- The term “analytical” is used for the analytical solutions in Eqs. (25) and (26) described in Sec. 3 when the non-dimensional function  $G(V^*)$  is obtained analytically for stretching-dominated deformation using the Mooney Rivlin hyperelastic potential as shown in Fig. 2.

For a representative bioelectronic device with a target delivery volume of  $V = 125 \mu\text{l}$  ( $V^* = 1.0$ ), flexible membrane of radius  $R_0 = 5 \text{ mm}$ , thickness  $h = 0.15 \text{ mm}$ , Young’s modulus  $E = 15 \text{ MPa}$ , and initial environmental pressure  $P_0 = 101.3 \text{ kPa}$ , the non-dimensional environmental pressure and microfluidic resistance are calculated as  $P_0^* = 0.225$  and  $M^* = 0.0015$ , respectively (all the parameters used to generate the volume temporal profiles are listed in Table 1). For this example, the target delivery volume of the flexible membrane is large enough to satisfy the stretching-dominated deformation condition in Eq. (4). Figure 3 shows the effect of increasing the initial gas volume  $V_0^*$  in delaying the delivery of the drug. When  $V_0^* = 0$  the solutions show excellent agreement on the entire delivery range. As  $V_0^*$  increases to 0.623, 1.256, and 1.880 the agreement remains over the entire volume temporal profile except at the beginning of the drug delivery process for times  $t^* < 0.1$  (Fig. 3(b)). Figure 3(b) shows that at the beginning of the drug delivery process, all the analytical solutions are stacked with each other up to  $t^* \sim 0.04$  because initially (when gas formation starts) the external pressure  $P_0$  exerted on the flexible membrane dominates Eq. (25), and it is independent of the initial gas volume  $V_0$ . Once sufficient gas has been generated from the electrochemical reaction, the dominant factor becomes the mechanics of the flexible membrane, i.e.,  $f(V)(V + V_0)$  dominates in Eq. (25), where the presence of  $V_0$  results in different total delivery times showed by the curves in Fig. 3(a). Figure 4 shows that, for a fixed volume (e.g.,  $V^* = 1.0$ ), the total delivery time is approximately linearly related to  $V_0^*$ , which is consistent with Eq. (24) for small  $M^*$ . The difference between the numerical and analytical solutions is less than 1%.

Figures 3 and 4 show that the presence of a non-zero  $V_0^*$  only delays the drug delivery (i.e., increase the total drug delivery time). Therefore, when  $P_0^*$  and  $M^*$  are fixed, the solution  $V_0^* = 0$  (electrolyte reservoir is filled) can be taken as the fastest delivery time achievable with the bioelectronic device. For example, if the drug must be delivered between two and four minutes, the limit  $V_0^* = 0$  can be designed to deliver the drug in two minutes and a non-zero  $V_0^* \neq 0$  can be used to deliver the drug in four minutes with the same bioelectronic device. Once the bioelectronic device is fabricated and ready to be used in animal experiments, only a few parameters can be changed during or before the drug delivery such as the electrical current  $i$  and the initial gas volume  $V_0$ . The electrolyte reservoir in Fig. 1 is refillable which allows the bioelectronic device to be used repeatedly. Therefore, by partially filling the electrolyte reservoir, the presence of an initial gas volume  $V_0$

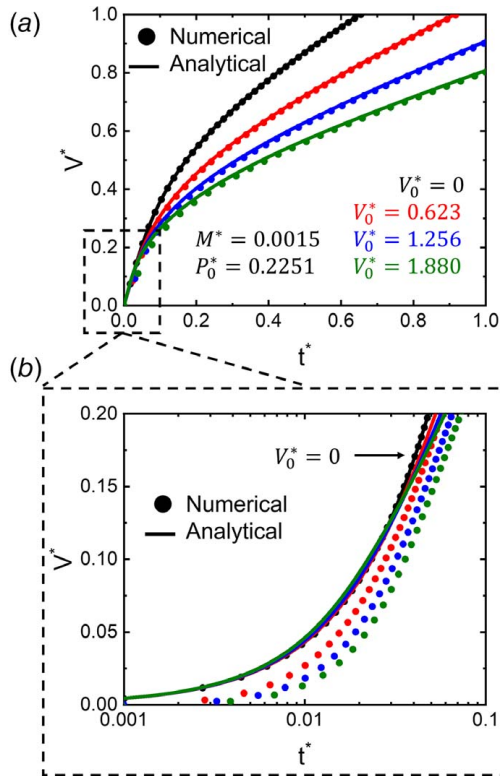


**Fig. 3** Effect of the initial gas volume in the drug volume temporal profile. (a) Drug delivery volume over time for  $V_0^* = 0, 0.623, 1.256,$  and  $1.880$  showing the delay effect for increasing  $V_0^*$ . (b) Zoom in of (a) at the initial time of delivery. The non-dimensional microfluidic resistance and environmental pressure are fixed to  $M^* = 0.0015$  and  $P_0^* = 0.2251$ .

can be used to control the drug delivery time without having to fabricate a new device with a different set of materials.

**4.1 Design Scalability for Small Animals, Large Animals, and Humans.** An advantage of these type of electrochemical bioelectronic devices is that the geometry can be scaled to tailored applications in small and large animals as well as humans by changing the three non-dimensional parameters in Eqs. (20)–(22) [19]. Figure 5 shows the dimensional volume temporal profiles for three representative device sizes with a target drug volume of  $3 \mu\text{l}$ ,  $125 \mu\text{l}$ , and  $1000 \mu\text{l}$  for experiments in small and large

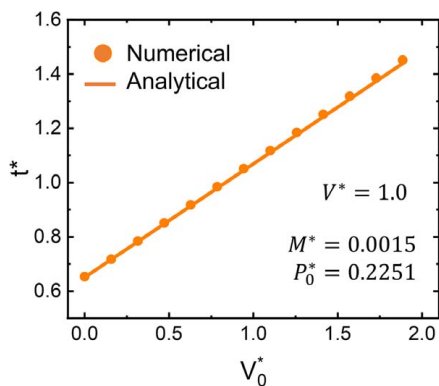


**Fig. 4** Effect of the initial gas volume in the total drug delivery time. The total delivery time for a fixed volume  $V^* = 1.0$  increases linearly with  $V_0^*$ . The non-dimensional microfluidic resistance and environmental pressure are fixed to  $M^* = 0.0015$  and  $P_0^* = 0.2251$ .

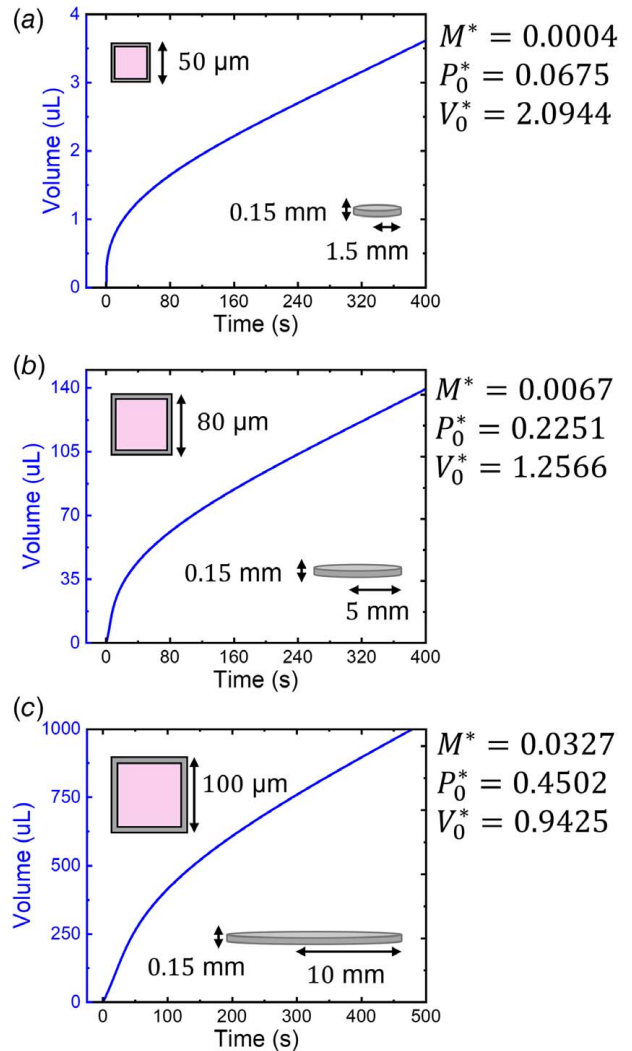


**Fig. 5** Representative examples of flexible membrane geometries. Design for (a) small animals, (b) large animals, and (c) humans showing the volume temporal profile. The unique combination of non-dimensional parameters is shown for each case.

animals where each configuration has a unique set of non-dimensional parameters based on the typical experimental parameters listed in Table 1. In all cases, the flexible membrane is modeled as a Mooney Rivlin incompressible solid with stretching-dominated deformation as explained in Sec. 2. The temporal profiles during delivery are very similar, only the magnitude of the target drug volume is different as shown in Fig. 5. To scale up the bioelectronic device from small animals to humans, the geometrical parameters such as  $R_0$  and the microfluidic cross-section  $a$  increase to accommodate larger volumes of drug inside the device reservoirs and deliver them in a timely fashion. Also, larger device geometries can accommodate different power strategies to deliver higher electrical currents to the interdigitated electrodes for a speedy drug delivery process. All these changes result in a unique combination of the three non-dimensional parameters. For the non-dimensional parameter  $V_0^*$  specifically, its value can be changed relatively easy as compared to the other two non-dimensional parameters since it is only related to the amount of initial gas present before the delivery.

**4.2 Radius of Flexible Membrane for Expedited Delivery.** For a target drug volume  $V$ , the delivery time decreases but approaches an asymptote as the radius of flexible membrane  $R_0$

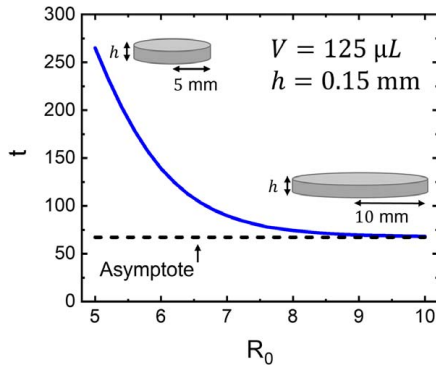


**Fig. 6 Optimization of the membrane radius for fast delivery.** For a representative fixed drug volume  $V = 125 \mu\text{L}$  used for delivery in large animal experiments, increasing  $R_0$  from 5 mm to 10 mm results in the largest decrease in delivery time. Further increasing the radius yields negligible results. Here,  $R_0$  changes while all the other parameters in the delivery are fixed. The initial gas volume  $V_0$  is taken as zero to speed up the delivery and the initial current  $i$  is fixed to 10 mA.

increases and  $f(V)$  becomes negligible, as deduced from Eq. (25).

$$t = \frac{4F}{3iRT} P_0 V + \frac{32\mu L V}{a^4 P_0} \quad (26)$$

Therefore, for a fixed drug volume  $V$ , increasing  $R_0$  can significantly decrease the delivery time before approaching the asymptote. However, the overall device size must be carefully considered when designing these bioelectronic systems as a large  $R_0$  can lead to bulky devices that pose bio-integration challenges in device securing or implantation strategies for epidermal or implantable applications, respectively. Figure 6 demonstrates that for a device with a drug volume  $V = 125 \mu\text{L}$ ,  $h = 0.15 \text{ mm}$  and  $R_0 = 5 - 10 \text{ mm}$ , the total delivery time for  $R_0 = 5 \text{ mm}$  is approximately  $t = 260 \text{ s}$ . When  $R_0 = 10 \text{ mm}$ , the delivery time is substantially reduced (by  $\sim 74\%$ ) to  $t = 68 \text{ s}$ , beyond this point further increasing the radius results in almost negligible improvement as it approaches the asymptote value given in Eq. (26).

**4.3 Alternative Material Models.** A similar approach to that described in Sec. 2 for a Mooney Rivlin solid can be applied to alternative material models, such as the Marlow hyperelastic potential [29] and a linear elastic relation between the true stress and logarithmic strain [19], to obtain the function  $f(V)$  analytically. The Marlow hyperelastic potential is shown since the mechanical response of the flexible membrane can be fitted directly from the nominal stress-strain data for a uniaxial, biaxial, or planar tests to obtain the  $f(V)$  curve from Eq. (8) as shown in our previous work [19]. For an incompressible, linear elastic relation between the true stress and logarithmic strain, the analytic  $f(V)$  is given by [19]

$$f(V) = \frac{64}{3\pi^3} \frac{Eh}{R_0^{10}(1-\nu)} V^3 \quad (27)$$

Figure 7 shows the influence of the material model in the drug delivery process where the corresponding normalized  $G(V^*)$  are shown in Fig. 7(a) for the linear elastic relation between the true stress and logarithmic strain and the Marlow hyperelastic potential for a flexible membrane with  $E = 15 \text{ MPa}$ ,  $R_0 = 5 \text{ mm}$ , and  $h = 0.15 \text{ mm}$ . All curves are the same for small drug volume  $V^* < 0.2$ . For  $V^* > 0.2$ , the curves are separated due to nonlinear deformation. The non-dimensional volume temporal profiles are shown in Fig. 7(b) where the numerical and analytical solutions agree well for a representative combination of the non-dimensional parameters  $M^* = 0.0015$ ,  $P_0^* = 0.2251$ ,  $V_0^* = 1.2566$ . The results show a clear distinction in the volume temporal profiles and drug

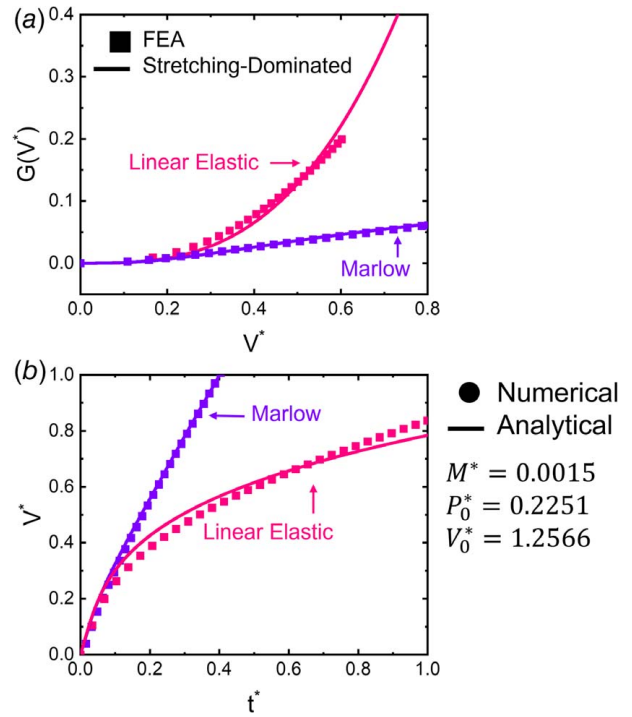


**Fig. 7 Modeling the flexible membrane with alternative material models.** (a) Normalized function  $G(V^*)$  for the flexible membrane modeled as a linear elastic relation between the true stress and logarithmic strain and as a Marlow hyperelastic incompressible solid. (b) volume temporal profiles during delivery for the representative non-dimensional parameters  $M^* = 0.0015$ ,  $P_0^* = 0.2251$  and  $V_0^* = 1.2566$ .

delivery time, which is related to the  $G(V^*)$  curves. For a non-dimensional volume of  $V^* = 1.0$  (corresponding to  $125 \mu\text{L}$  of drug), the Marlow model yields  $\sim t^* = 0.4$  which is equivalent to approximately  $t = 116 \text{ s}$ , while the linear elastic relation between the true stress and logarithmic strain predicts almost ten times longer at a delivery time of  $t = 965 \text{ s}$ .

## 5 Conclusions

In summary, this work presents the analytical model for drug delivery time using bioelectronic devices while accounting for the effect of the initial gas volume present in the electrochemical reservoir before the delivery process. The drug delivery process is controlled by three non-dimensional parameters: the normalized environmental pressure, the initial gas volume, and the microfluidic resistance which can be scaled from small animal studies to large animal and human trials following unique combinations of the non-dimensional parameters. The analytic model, detailed analysis of the non-dimensional parameters related to the initial gas volume, and volume temporal profile results are important to guide parametric optimization of these devices for refillable/repeated studies and obtain the estimated total delivery time for localized drug delivery studies.

## Acknowledgment

R.A. and J.L.C. acknowledge support from the National Science Foundation Graduate Research Fellowship (NSF Grant No. DGE-1842165). R.A. also acknowledges funding from the Ford Foundation Predoctoral Fellowship. J.L.C., A.V.G., Y.Z., and J.A.R. acknowledge the support of the HEAL Initiative of the National Institutes of Health under award number UG3DA050303. The conclusions, opinions and other statements

in this publication are the authors' and not necessarily those of the sponsoring institution.

## Conflict of Interest

There are no conflicts of interest.

## Data Availability Statement

The datasets generated and supporting the findings of this article are obtainable from the corresponding author upon reasonable request. The authors attest that all data for this study are included in the paper. No data, models, or code were generated or used for this paper.

## References

- [1] Jeong, J. W., McCall, J. G., Shin, G., Zhang, Y., Al-Hasani, R., Kim, M., Li, S., Sim, J. Y., Jang, K. I., Shi, Y., Hong, D. Y., Liu, Y., Schmitz, G. P., Xia, L., He, Z., Gamble, P., Ray, W. Z., Huang, Y., Bruchas, M. R., and Rogers, J. A., 2015, "Wireless Optofluidic Systems for Programmable In Vivo Pharmacology and Optogenetics," *Cell*, **162**(3), pp. 662–674.
- [2] Spieth, S., Schumacher, A., Holtzman, T., Rich, P. D., Theobald, D. E., Dalley, J. W., Nouna, R., Messner, S., and Zengerle, R., 2012, "An Intra-Cerebral Drug Delivery System for Freely Moving Animals," *Biomed. Microdevices*, **14**(5), pp. 799–809.
- [3] Gensler, H., Sheybani, R., Li, P. Y., Mann, R. L., and Meng, E., 2012, "An Implantable MEMS Micropump System for Drug Delivery in Small Animals," *Biomed. Microdevices*, **14**(3), pp. 483–496.
- [4] Zhang, Y., Mickle, A. D., Gutruf, P., McIlvried, L. A., Guo, H., Wu, Y., Golden, J. P., Xue, Y., Grajales-Reyes, J. G., Wang, X., Krishnan, S., Xie, Y., Peng, D., Su, C. J., Zhang, F., Reeder, J. T., Vogt, S. K., Huang, Y., Rogers, J. A., and Gereau, R. W., 2019, "Battery-Free, Fully Implantable Optofluidic Cuff System for Wireless Optogenetic and Pharmacological Neuromodulation of Peripheral Nerves," *Sci. Adv.*, **5**(7), pp. 1–12.
- [5] Zhang, Y., Castro, D. C., Han, Y., Wu, Y., Guo, H., Weng, Z., Xue, Y., Ausra, J., Wang, X., Li, R., Wu, G., Vázquez-Guardado, A., Xie, Y., Xie, Z., Ostojich, D., Peng, D., Sun, R., Wang, B., Yu, Y., Leshock, J. P., Qu, S., Su, C. J., Shen, W., Hang, T., Banks, A., Huang, Y., Radulovic, J., Gutruf, P., Bruchas, M. R., and Rogers, J. A., 2019, "Battery-Free, Lightweight, Injectable Microsystem for in Vivo Wireless Pharmacology and Optogenetics," *Proc. Natl. Acad. Sci. U. S. A.*, **116**(43), pp. 21427–21437.
- [6] Kumar, A., and Pillai, J., 2018, "Implantable Drug Delivery Systems: An Overview," *Nanostructures for the Engineering of Cells, Tissues and Organs*, Alexandru Mihai Grumezescu, ed., William Andrew Publishing, Cambridge, MA, pp. 473–511.
- [7] Koo, J., Kim, S. B., Choi, Y. S., Xie, Z., Bandodkar, A. J., Khalifeh, J., Yan, Y., et al., 2020, "Wirelessly Controlled, Bioresorbable Drug Delivery Device with Active Valves That Exploit Electrochemically Triggered Crevice Corrosion," *Sci. Adv.*, **6**(35), p. eabb1093.
- [8] Qazi, R., Yeon Kim, C., Kang, I., Binazarov, D., McCall, G., and Jeong, J., and W, J., 2020, "Implantable Optofluidic Systems for Wireless In Vivo Photopharmacology," *ChemPhotoChem*, **5**, pp. 96–105.
- [9] Vargason, A. M., Anselmo, A. C., and Mitragotri, S., 2021, "The Evolution of Commercial Drug Delivery Technologies," *Nat. Biomed. Eng.*, **5**(9), pp. 951–967.
- [10] Villarruel Mendoza, L. A., Scilletta, N. A., Bellino, M. G., Desimone, M. F., and Catalano, P. N., 2020, "Recent Advances in Micro-Electro-Mechanical Devices for Controlled Drug Release Applications," *Front. Bioeng. Biotechnol.*, **8**, pp. 1–28.
- [11] Stewart, S. A., Domínguez-Robles, J., Donnelly, R. F., and Larrañeta, E., 2018, "Implantable Polymeric Drug Delivery Devices: Classification, Manufacture, Materials, and Clinical Applications," *Polymers*, **10**(12), p. 1379.
- [12] Bußmann, A. B., Grünerbel, L. M., Durasiewicz, C. P., Thalhofer, T. A., Wille, A., and Richter, M., 2021, "Microdosing for Drug Delivery Application—A Review," *Sens. Actuators, A*, **330**, p. 112820.
- [13] Laracuente, M. L., Yu, M. H., and McHugh, K. J., 2020, "Zero-Order Drug Delivery: State of the Art and Future Prospects," *J. Controlled Release*, **327**, pp. 834–856.
- [14] Stearns, L. J., Narang, S., Albright, R. E., Hammond, K., Xia, Y., Richter, H. B., Paramanandam, G. K., Haagenson, K. K., and Doth, A. H., 2019, "Assessment of Health Care Utilization and Cost of Targeted Drug Delivery and Conventional Medical Management vs Conventional Medical Management Alone for Patients With Cancer-Related Pain," *JAMA Netw. Open*, **2**(4), p. e191549.
- [15] Chen, Y., Rommelfänger, N. J., Mahdi, A. I., Wu, X., Keene, S. T., Obaid, A., Salleo, A., Wang, H., and Hong, G., 2021, "How Is Flexible Electronics Advancing Neuroscience Research?," *Biomaterials*, **268**, p. 120559.
- [16] Gensler, H., Sheybani, R., Li, P., Lo, R., Zhu, S., Yong, K., Prasad, P. N., Masood, R., Sinha, U. K., and Meng, E., 2010, "Implantable MEMS Drug Delivery Device For Cancer Radiation Reduction," 2010 IEEE 23rd International Conference on Micro Electro Mechanical Systems (MEMS), Hong Kong, China, Jan. 24–28.
- [17] Rosenblum, D., Joshi, N., Tao, W., Karp, J. M., and Peer, D., 2018, "Progress and Challenges Towards Targeted Delivery of Cancer Therapeutics," *Nat. Commun.*, **9**(1), p. 1410.
- [18] Cobo, A., Sheybani, R., Tu, H., and Meng, E., 2016, "A Wireless Implantable Micropump for Chronic Drug Infusion Against Cancer," *Sens. Actuators, A*, **239**, pp. 18–25.
- [19] Avila, R., Li, C., Xue, Y., Rogers, J. A., and Huang, Y., 2021, "Modeling Programmable Drug Delivery in Bioelectronics with Electrochemical Actuation," *Proc. Natl. Acad. Sci. U. S. A.*, **118**(11), p. e2026405118.
- [20] Stanczyk, T., Ilic, B., Hesketh, P. J., and Boyd IV, J. G., 2000, "Microfabricated Electrochemical Actuator for Large Displacements," *J. Microelectromech. Syst.*, **9**(3), pp. 314–320.
- [21] Pang, C., Tai, Y. C., Burdick, J. W., and Andersen, R. A., 2006, "Electrolysis-Based Diaphragm Actuators," *Nanotechnology*, **17**(4), pp. 64–68.
- [22] Lee, D. E., Soper, S. A., and Wang, W., 2010, "Fabrication and Mathematical Analysis of an Electrochemical Microactuator (ECM) Using Electrodes Coated with Platinum Nano-Particles," *Microsyst. Technol.*, **16**(3), pp. 381–390.
- [23] Ashraf, M. W., Tayyaba, S., and Afzulpurkar, N., 2011, "Micro Electromechanical Systems (MEMS) Based Microfluidic Devices for Biomedical Applications," *Int. J. Mol. Sci.*, **12**(6), pp. 3648–3704.
- [24] Urone, P. P., and Hinrichs, R., 2012, "College Physics," *College Physics*, OpenStax, Houston, Texas, pp. 465–466.
- [25] Beebe, D. J., Mensing, G. A., and Walker, G. M., 2002, "Physics and Applications of Microfluidics in Biology," *Annu. Rev. Biomed. Eng.*, **4**(1), pp. 261–286.
- [26] Pardo, G. C., and Hagen, R. L., 1972, "Symmetrical Bending of Circular Plates Using Finite Elements," *Comput. Struct.*, **2**(4), pp. 547–553.
- [27] Mooney, M., 1940, "A Theory of Large Elastic Deformation," *J. Appl. Phys.*, **11**(9), pp. 582–592.
- [28] Avila, R., Wu, Y., Rogers, J. A., and Huang, Y., 2021, "A Mechanics Model for Injectable Microsystems in Drug Delivery," *J. Mech. Phys. Solids*, **156**, p. 104622.
- [29] Marlow, R. S., 2003, "A General First-Invariant Hyperelastic Constitutive Model," *Constitutive Models For Rubber – Proceedings Constitutive Models for Rubber*, London, UK, Sept. 15–17, pp. 157–160.
- [30] Kumar, M., 2011, "Methods for Solving Singular Perturbation Problems Arising in Science and Engineering," *Math. Comput. Model.*, **54**(1–2), pp. 556–575.
- [31] Cameron, C. G., and Freund, M. S., 2002, "Electrolytic Actuators: Alternative, High-Performance, Material-Based Devices," *Proc. Natl. Acad. Sci. U. S. A.*, **99**(12), pp. 7827–7831.
- [32] Feiner, A. S., and McEvoy, A. J., 1994, "The Nernst Equation," *J. Chem. Educ.*, **71**(6), pp. 493–494.
- [33] Silbey, R. J., Alberty, R. A., and Bawendi, M. G., 2004, "Physical Chemistry," *Physical Chemistry*, John Wiley & Sons, pp. 17–21.